City, University of London Institutional Repository

Fiber Bragg grating sensor Investigation on Bond Stress of Steel-carbon Fiber Reinforced Concrete

Lei Wang[a], Junwen Chen[a], Ni Shen[a] Feng Fu[b,a*]

[a] Guilin University of Technology School of civil and architectural engineering, Guilin 541004, China

[b] School of Mathematics, Computer Science and Engineering, City, University of London

Abstract： Understanding the bonding stress distribution and reinforcement strain distribution between steel-carbon fiber composite bars (SFCB) and concrete is essential to the design of the new SFCB reinforced concrete. However, currently, the bond stress and reinforcement strain distribution patterns of SFCB concrete are not clear. Therefore, this paper carries out a series of pull-out tests on SFCB reinforced concrete and other two reinforcement and CFRP reinforced concrete. With the help of a new technology--fiber Bragg grating sensing technology, the reinforcement strain and bonding stress distribution between SFCB and concrete are studied. The results show that for all 3 types of specimens, the bond stress between reinforcement and concrete is neither uniformly distributed nor reduced linearly along the bond length. For the SFCB reinforcement, the steel core strain value is less than the carbon fiber strain value at the same position. Based on the test results, the bonding stress model and the bond stress distribution model are established. The two models agree well with the test data and can be used to predict the bond stress and bond stress distribution.

Key words: SFCB; pull out test; bond stress distribution; strain; fiber Bragg grating sensing technology

1.Introduction

Steel-FRP composite reinforcement (SFCB) is a newly developed reinforcing bar, it is manufactured

---

by wrapping steel bars with FRP as the outer layer material combines the advantages of high elastic modulus and good ductility of ordinary steel bars, as well as the advantages of strong corrosion resistance and high ultimate strength of FRP, which can effectively solve the problems of corrosion of steel bars in concrete and brittle failure of fiber reinforced plastic materials (Zheng BL, Li W, Zhang WW et al. (2004) Mechanics Behavior of FRP Wrapped Rebar Reinforced Concrete Ⅱ: Mechanic Tests. Acta Materiae Compositae Sinica 21(3):79-83. Wu G, Luo YB, Wu ZS et al. (2010) Experimental and Theoretical Studies on the Mechanical Properties of Steel-FRP Composite Bars. China Civil Engineering Journal 43(03):53-61.Sun ZY, Tang Y, Luo YB et al. (2017) Mechanical Properties of Steel-FRP Composite Bars under Tensile and Compressive Loading. International Journal of Polymer Science 2017(1):5691278-1-5691278-11.

In recent years, an increasing number of scholars have studied the mechanical properties of SFCB and SFCB concrete members (Zhang LL (2011) Study on Bond Behavior between Steel-FRP Composite Bar (SFCB) and Concrete under Cyclic Loading. MSc thesis,Southeast University, Nanjing city, Jiangsu province, China (in Chinese).Malvar L J, Cox J V and Cochran K B (2003) Bond between Carbon Fiber Reinforced Polymer Bars and Concrete I:Experimental Study. Journal of Composites for Construction 7(2):154-163.L. J. Malvar, N. R. Joshi,J. A. Beran et al. (2003) Environmental Effects on the Short-Term Bond of Carbon Fiber-Reinforced Polymer (CFRP) Composites. Journal of Composites for Construction 7(1):58-63.Wang L , Zhang JW , Huang CS et al. (2020) Comparative Study of Steel-FRP, FRP and Steel-Reinforced Coral Concrete Beams in Their Flexural Performance. Materials 13(9)：2097.Wang L, Zhang JW, Chen W et al. (2020) Short term crack width prediction of CFRP bars reinforced coral concrete. Engineering Structures 218(Sep.1)：110829.1-110829.12.) Research by PanPan J (2016) Research progress on fabrication technique and tensile performance of FRP-Steel composite bar. Journal of Civil

and Environmental Engineering 38(S2):18-20., XuXu YQ (2015) Resarch on Basic Properties of Steel Fiber Composite Bars Reinforced Marine Sand Concrete Beams. MSc thesis,Southeast University Nanjing city, Nanjing city, Jiangsu province, China (in Chinese).and others showed that the elastic modulus of a SFCB is effectively improved compared with single FRP reinforcement, the steel bar has stable secondary stiffness after yielding, and the stress-strain relationship curve presents a double-fold line characteristics: during the loading process, before the steel bar core of SFCB yields, the stress increases linearly with the strain; when the steel bar core yields, the stress continues to increase linearly with the strain due to the existence of wrapped fibers, but the slope decreases. At the same time, SFCBs have good ductility and shear performance, and SFCB reinforced concrete structures can effectively improve the bearing capacity and stiffness of the a structure. Experiments by Mohamed F. M. Fahmy et al.Fahmy M F M , Abd-Elshafy Z E , Wu Z . (2017) Experimental and Numerical Evaluation of the Shear Behavior of Reinforced Concrete T-Beams with Hybrid Steel-FRP Stirrups. Journal of Composites for Construction 21(4):04017007.1-04017007.18. showed that compared with conventional RC beams, concrete beams rein forced with steel-FRP stirrups successfully showed a considerable increase in the beam shear strength and deformability.

At present, only limited research has been done on the bond performance between SCFCBs and concrete. According to Sun's research, in general(Sun ZY, Wu G, Wu ZS et al. (2009) Experimental Study on the Bond Behavior between Steel Fiber Composite Bar (SFCB) and Concrete. Earthquake Resistant Engineering and Retrofitting 31(01):21-27.Shi LZ, Zhang JR (2014) Experimental Study on Anchorage Performance of Chemical Adhesive Steel Bar in Concrete. Applied Mechanics & Materials 578-579(2014):331-334.), the bond failure between reinforcement and concrete is mainly manifested in three modes: concrete splitting, reinforcement pulling out and reinforcement fracture. The tensile strength of fiber reinforced concrete

is higher, and the bond strength with concrete is weaker than that with steel bar under the same conditions. Therefore, the former two failure modes of fiber reinforced concrete are quite common, and reinforcement fracture of reinforcement is rare. However, with the existence of a steel core, the splitting and pulling-out failure modes of SFCB-concrete bonded specimens can be subdivided into two cases: pre-yield failure and post-yield failure. In Wang's research (Wang L, Shen N, Zhang MM et al. (2020) Bond performance of Steel-CFRP bar reinforced coral concrete beams. Construction and Building Materials 245(Jun.10): 118456.1-118456.11.) , four characteristic points in the bond-slip curve between SFCBs and coral concrete were analysed, and a bond-slip model that can accurately describe the bond-slip between SFCBs and concrete was established. Compared with the study of bond performance between FRP bars and concrete, general understanding of the bond behaviour between a SFCB and concrete is lacking. Thus, structural calculations, such as assessments of the damage mechanisms, behaviour control and many other aspects of SFCB concrete, are required. Although the establishment of the bond stress-slip constitutive relation in most studies at present assumes that the stress of the reinforcement is uniformly distributed along the embedded length, in fact, there are different bond-slip relations between reinforcement and concrete at different positions of buried length (Gu XL, Chen ZY and Farhad Ansari (2000) Embedded Fiber Optic Crack Sensor for Reinforced Concrete Structures. Structural Journal 97(3): 468-476.Jiang TY, Fang Z (2010) Bond Stress Distribution of CFRP Tendon in Reactive Powder Concrete. China Journal of Highway and Transport 23(01):49-57.). Obviously, understanding the distribution law of the bond stress between the reinforcement and concrete would be very be helpful for understanding the bond performance between the reinforcement and concrete. In their research, Xu et al.Xu YL, Shen WD and Wang H (1994) An Experimental Study of Bond-Anchorage Properties of Bars in Concrete. Journal of Building Structures 1994(03):26-37. pointed out that the bond stress-slip constitutive relation between the reinforcement and concrete changes at different anchorage

4

positions and established a curve equation of the bond anchorage constitutive relation including position parameters and critical eigenvalue of the bond stress. Danying Gao et al.Gao D, Huang Y, Chen G et al. (2020) Bond stress distribution analysis between steel bar and steel fiber reinforced concrete using midpoint stress interpolation method. Construction and Building Materials 260:119866. analyzes the strain of reinforcement, obtains the bond stress distribution curve under different pulling loads, and proposes the local bond test stress prediction model of high strength reinforcement and steel fiber concrete. Pan WH et al.Pan WH , Tao MX , Nie X et al. (2018) Rebar Anchorage Slip Macromodel Considering Bond Stress Distribution: Monotonic Loading and Model Application. Journal of Structural Engineering 144(8):04018097.presented a modified macromodel for calculating the anchorage slip of rebar under monotonic loading. The proposed macromodel reflects the bond stress distribution along rebar and hence captures slip responses over the entire rebar stress range. Hyeon-Jong Hwang et al.Hwang H J , Park H G , Yi W J et al. (2017) Development Length of Standard Hooked Bar Based on Non-Uniform Bond Stress Distribution. ACI Structural Journal 114(6) : 1637-1648.proposed a heterogeneous bond stress distribution model considering the hook-anchor effect to predict the developmental length or the average bond stress of the reinforcement. Because a SFCB is a composite reinforced material, the bond between the SFCB and concrete is affected by two bonding interfaces: "fiber-concrete" and "fiber-steel core". Therefore, the study of bonding performance and bonding stress distribution between a SFCB and concrete is far more complicated than that of single reinforced material.

When we study the bond-slip constitutive relation, it is generally assumed that the bond stress is uniformly distributed in the bond length, and the average bond stress is used instead of the bond stress at each position. However, the actual bond stress at different positions of the bond length is different. In the area with bond force, the bond force starts to be large, reaches the maximum value after a certain length,

and then gradually decreases until it is zero. The research of Zhao et al. Zhao WL, Yao ZB, Yu QB et al. (2019) Experimental Study on Bond Anchorage Behavior between Deformed Steel Bar and Lightweight Concrete. Building Structure 49(04):70-75. results showed that the slope of the steel bar stress curve is more obvious for specimens with a bond length of 160 mm than for specimens with a bond length of 80 mm, and the bond stress at different points in the bond length is quite different. The distribution area of bond stress is high stress area, which is generally higher than the average bond stress. Jiang et al.Jiang TY, Fang Z (2007) Bond Stress Distribution of Bond-type Anchors for CFRP Tendons under the Ultimate Tensile Capacity. Journal of Highway and Transportation Research and Development 2007(12):75-78 92. optimized the model by determining the boundary conditions and obtained a smooth and continuous bond stress distribution curve model; Through theoretical analysis, Liu Liu YH, Yuan Y. (2011) Bond Stress Distribution Model of Full-thread GFRP Bars in Concrete. Chinese Journal of Underground Space and Engineering 7(S1):1353-1356+1363. proposed a two-stage simplified distribution model of bond stress including slip sections and non-slip sections. Although it is assumed that there is a certain gap between the stress distribution of reinforcement along the length direction and the actual situation, when the bonding length is short, it can still reflect the bonding strength and performance between them (Wang L, Shen N, Zhang MM et al. (2020) Bond performance of Steel-CFRP bar reinforced coral concrete beams. Construction and Building Materials 245(Jun.10): 118456.1-118456.11.). The measuring point spacing of fiber Bragg grating (FBG) can be set freely, which can provide a shorter calculated bonding length, thus reflecting the bonding performance more truly. Fiber Bragg Grating (FBG) produces a small periodic distribution by changing the refractive index of the fiber core. When broadband light waves are transmitted in the grating, the incident light will be reflected back at the corresponding wavelength, while the rest of the transmitted light will not be affected, so the FBG plays the role of light wave selection. At the same

time, due to the close bonding between the grating and the reinforcement, there is no relative slip at the interface between the grating and the reinforcement in a certain range. When the reinforcement in the area where the bare fiber Braag grating is bonded in the reinforcement changes in strain or temperature, the grating and the reinforcement at the bonding place are subjected to force changes synchronously, thus causing the modulation period of the grating to change, and directly or indirectly converting the measured reinforcement changes into strain or temperature changes on the fiber grating. Thereby causing the change of the central wavelength of the fiber Bragg grating. By calibrating the relationship between the change of the central wavelength of the fiber Bragg grating and the strain and temperature, the value of the measured physical quantity can be calculated from the change of the central wavelength of the grating (Zhang MM (2019) Experimental study on the bonding properties of steel-carbon fiber composite bars with all-coral concrete. MSc thesis,Guilin University of Technology,Guilin city, Guangxi province, China (in Chinese).Huang X, Jin ZK and Shen Q (2021) New Method of Temperature and Strain Decoupling Based on Directivity of Fiber Bragg Grating Sensing. Journal of Physics: Conference Series 2101(1):19-20. HILL K.O, MELTZ G. (1997) Fiber Bragg grating technology fundamentals and overview. Journal of Lightwave Technology: A Joint IEEE/OSA Publication 15(8):1263-1276.Tang GN (2013) Application study on FBG sensor applied to hull structure health monitoring. MSc thesis,Wuhan University of Technology, Wuhan city, Hubei Province, China (in Chinese).) . Therefore, the strain can be measured more accurately by using the fiber Bragg grating.

In summary, the above research on bond stress distribution of steel bars and CFRP bars remains limited, in addition, the research on the bond stress distribution between SFCBs and concrete is still rare. Therefore, based on the existing research foundation of steel bars and CFRP bars, this paper adopts a new technology: fiber Bragg grating sensing technology to carry out experimental research on the distribution

law of steel strain and bond stress in SFCB concrete. These research results can provide a reference for the research of bond performance between SFCBs and concrete.

2. Test Program

2.1 Test materials

The strength of the concrete prepared in this paper is C80. The test uses P•O 52.5 grade ordinary Portland cement, the coarse aggregate is 5~20 mm continuous graded ordinary crushed stone, the fine aggregate is ordinary river sand with a fineness modulus of 2.75, the water absorption is 0.9 %, and the mixing water is used as domestic water. Polycarboxylic acid superplasticizer with a water reduction rate of approximately 20 % is mixed, and the mixing amount is 0.2 % of the mass of the cementing materials. The concrete mix ratio and basic mechanical parameters are shown in Table 1.

The test bars for the SFCBs (composed of a crescent-shaped steel core and a CFRP layer), the CFRP bars produced by China Jiangsu Intellectual Science and Technology Nantong Co., Ltd. and the crescent-shaped steel bars produced by China Guangxi Liuzhou Steel Group Co Ltd are shown in Fig.1.The apparent parameters and mechanical properties of the bars are shown in Table 2.

The type of fiber Braag grating used in the experiment is single-mode fiber, the number of Braag gratings on each fiber is 3, the grating length of the fiber grating is 10 mm, and the center wavelengths of the three gratings are 1530 nm, 1545 nm and 1555 nm in turn.

Fig. 1. Test bars.

Table 1. Concrete mix ratio and basic mechanical performance parameters.

Water cement ratio	Cement (kg/m³)	Fly ash (kg/m³)	Mineral powder (kg/m³)	Sand (kg/m³)	Coarse aggregate (kg/m³)	Water (kg/m³)	Water reducer (kg/m³)	Cube Compressive strength (MPa)	Axial compressive strength (MPa)	Tensile splitting strength (MPa)	Young's Modulus (GPa)
0.27	404	69	104	720	1100	156	1.731	83.2	53.5	5.3	39.8

Table 2. Mechanical properties of bars.

Bar Type	Bar diameter (mm)	Steel core diameter (mm)	Rib height (mm)	Rib width (mm)	Rib spacing (mm)	Yield strength (MPa)	Bar Young's Modules (GPa)	Ultimate strength (MPa)	Outer fibre Young's Modules (GPa)	Steel core Young's Modules (GPa)
SCFRP	14	8	0.55	10.41	13.37	344.8	150.2	1102.3	127.3	197.4
CFRP	14	—	1.22	10.28	13.84	—	131.6	1102.3	—	—
steel bar	14	—	1.11	2.89	8.35	393.2	205.0	644.4	—	—

9

2.2 Specimen design

The bond lengths of the SFCB pull-out specimens are designed to be 70 mm and 112 mm, and the bond lengths of the CFRP bars and steel bar pull-out specimens are designed to be 70 mm. The bond centre pull-out specimens are made according to the Canadian Standards Association (CSA) standard Canadian Standard Association (2002) CSA S806 02 Design and construction of building components with fiber reinforced polymers. Toronto, Canada: Canadian Stands Association International., with a size of 150×150×150 mm. In order to avoid local extrusion of the concrete at the loading end, PVC sleeves are set at the unbonded section of the specimen to isolate the reinforcement from the concrete and adjust the bonding length, as shown in Fig.2. One end of SFCB was stripped of 75 mm carbon fiber, and the steel core was exposed, which was bonded with a 250 mm steel casing at the clamping end, so as to ensure that the stress of the composite reinforcement and the steel core at the end was synchronous during the test loading. For the specimen number is A-B-C80, A represents the type of reinforcement (where SF stands for the SFCB concrete specimen, C stands for the CFRP reinforced concrete specimen, and S stands for the reinforced concrete specimen), and B stands for the bond length.

In the experiment, fiber Bragg grating sensors are used to test and collect the strain of the reinforcement. After each reinforcement is grooved, the fiber Bragg grating is aligned with measuring points that are evenly distributed on the bonding length and adhered to the steel core and fiber surface in the groove (three gratings are arranged on one fiber, two fibers are arranged on each steel bar and CFRP bar, and four fibers are arranged on each SFCB) , as shown in Fig.3. The embedded physical drawing of fiber grating is shown in Fig.4. During the test, the fiber grating is connected to the demodulator as a probe, and the grating is stressed synchronously with the tensioned longitudinal bar. When the external load is applied, the photoelastic effect causes the refractive index of the fiber grating to change, and the

deformation causes the grating area to change, which is reflected to the demodulator for display through the wavelength change. Finally, the wavelength change of the measuring point grating area under the load is converted into the strain solution of each measuring point of the tensioned longitudinal bar.
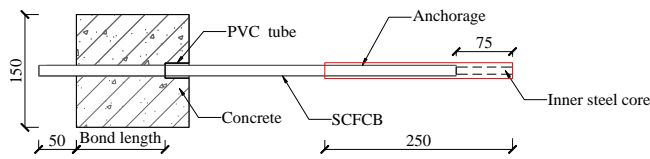

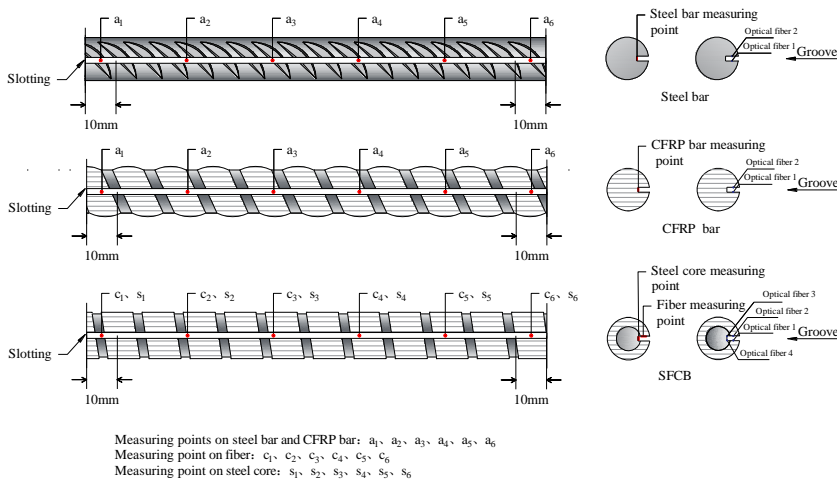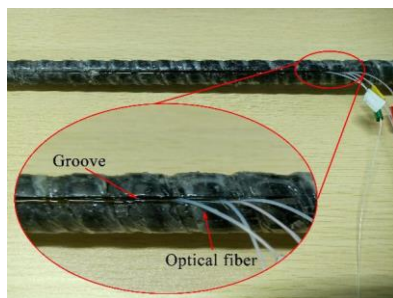**Fig. 2.Schematic diagram of the specimens.**

Measuring points on steel bar and CFRP bar：a_1、a_2、a_3、a_4、a_5、a_6
Measuring point on fiber：c_1、c_2、c_3、c_4、c_5、c_6
Measuring point on steel core：s_1、s_2、s_3、s_4、s_5、s_6

Fig. 3. Fiber Bragg grating measuring point layout.

11

Fig.4. Physical drawing of fiber grating embedding

2.3 Pull-out tests set-up

As shown in Fig. 5, the centre pull-out test is carried out on a universal hydraulic testing machine,

the maximum loading capacity of universal hydraulic testing machine is 1000 kN and the pull-out load

loading rate is 0.5 mm/min. The loading device consists of four high-strength bolts, two angle steels and

a square steel plate, and the centre of the square steel plate is provided with an alignment hole with a

diameter of 20 mm to avoid eccentric stress on the specimen. The test ends when there is a fracture of

reinforcement or a splitting of the concrete during the test.

<table>
<tr><td>1</td><td>Universal hydraulic testing machine</td></tr>
<tr><td>2</td><td>High strength friction grip bolt</td></tr>
<tr><td>3</td><td>Angle steel</td></tr>
<tr><td>4</td><td>Nut</td></tr>
<tr><td>5</td><td>Square steel plate</td></tr>
<tr><td>6</td><td>Fixture</td></tr>
<tr><td>7</td><td>PVC tube</td></tr>
<tr><td>8</td><td>Test bar</td></tr>
<tr><td>9</td><td>Anchorage</td></tr>
</table>

Fig. 5. Schematic diagram of pull-out test equipment.

3. Test results and analysis

3.1 Bond failure mode

In this paper, because the thickness of the concrete protective layer of SFCB bonded specimens is

relatively thin, the test phenomenon is mainly concrete splitting failure before steel bar yielding. All steel

bar bonded specimens exhibit steel bar tensile failure, while CFRP bar bonded specimens exhibit concrete

Commented [MN1]: Please mention the model of the UTM and/or maximum   loading capacity.

splitting failure. When the bond failure occurs between the reinforcement and concrete, the interface failure mode is affected by the shear strength of the reinforcement. In this experiment, the strength of the fiber and resin matrix on the surface of CFRP reinforcement and SFCB is low, and scraping failure easily occurs when they slip relative to concrete. Therefore, at the bond interface between reinforcement and concrete, the extrusion interface between the transverse ribs on the surface of the reinforcement and concrete exhibits obvious wear. In addition, due to the high strength of concrete, there is less damage to concrete at the bonding interface, and there are clear outline marks of reinforcement and a small amount of fiber powder, as shown in Figure 6.

(a) C-5d-C80

(b) SF-8d-C80

Fig. 6. Failure mode of bond.

3.2 SFCB strain distribution

An SFCB is a composite of two materials, and the tensile stress of the steel core is actually transmitted

through carbon fiber, so it is very important to maintain the deformation coordination between them. It can be seen from Fig. 7 that with the increase of load, the growth trend and growth rate of steel core strain and outer carbon fiber strain at each measuring point are basically the same, but with the increasing of load, the steel core strain is smaller than the carbon fiber strain at the same position.

In the central pull-out test, the tensile stress of the reinforcement at the loading end is the largest, and the load is gradually transferred to the concrete through bonding action, and the stress of the reinforcement at the free end is zero. Therefore, in the whole bonding interval, the tensile strain of the reinforcement decreases from the loading end to the free end, and the first half near the loading end decreases rapidly, while the change in the second half gradually slows down. At the same time, the specimens with different reinforcement types and different bond lengths show obvious differences. Under the same bonding conditions, influenced by the elastic modulus of the materials, under the same load, the tensile strain of the CFRP bars is greater than that of the SFCB, and the strain of the steel bars is the smallest, and the difference gradually increasing with the increase of the load, as shown in Fig. 8. The loading end strain of the SCFCB is able to increase by approximately 40% over normal reinforcement. Bond length affects the change trend of strain curve. The shorter the bond length is, the faster the strain curve decreases, as shown in Fig.9.
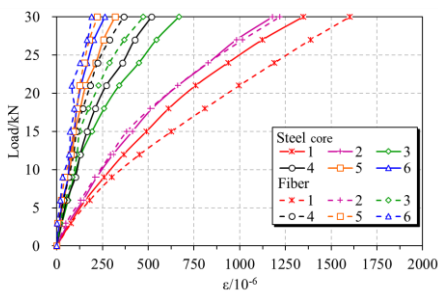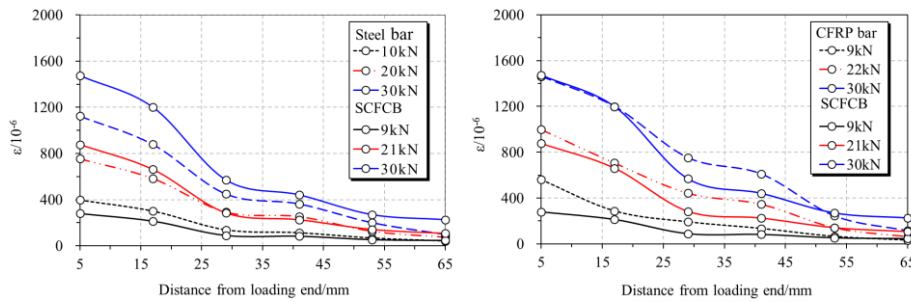

(a)Load-strain curve of SF-5d-C80   (b)Load-strain curve of SF-8d-C80
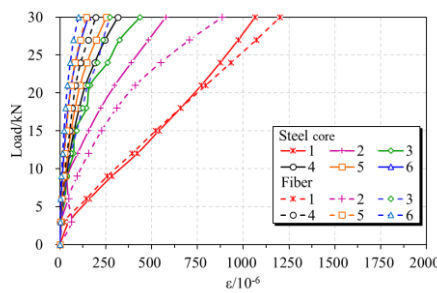
14

Fig. 7. Load-strain curve of SFCB steel core and outer fiber.

Note: The positions of the measuring points are set according to Fig. 3. From the loading end to the free end, the measuring point numbers are 1, 2, 3, 4, 5 and 6 in turn.

(a)Comparison between SFCB and steel bars   (b)Comparison between SFCB and CFRP bars

Fig. 8. Influence of reinforcement type on strain distribution.
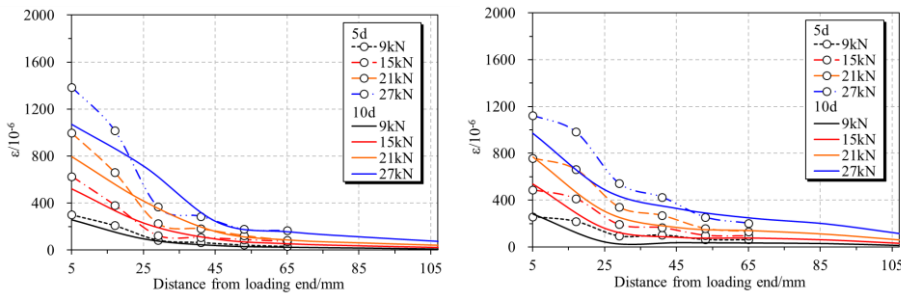
(a)SFCB steel core strain   (b)SFCB outer carbon fiber strain

Fig. 9. Influence of bond length on strain distribution.

4 Calculation model of bond stress of SFCB concrete

Based on the test results calculation models for both the bond stress and bond stress distribution are developed in this paper. The bond stress caused by the relative deformation between reinforcement and concrete is usually composed of chemical adhesion, friction and bearing action (Sun ZY, Tang Y, Luo

YB et al. (2017) Mechanical Properties of Steel-FRP Composite Bars under Tensile and Compressive

Loading. International Journal of Polymer Science 2017(1):5691278-1-5691278-11. Wang B, Bai GL, Li

J et al. (2012) Experimental and the Theoretical Analysis of Bond Stress Distribution Between the Rebar

and the Recycled Concrete. Industrial Construction 42(04):10-14.). It is difficult to measure or strictly

distinguish the components of bond stress separately. At present, most of them are calculated indirectly

according to the strain and stress changes of reinforcement along the bond length. As shown in Fig.

10(a), the stresses at both ends of the unit body are unequal, and the stress difference is balanced by the

surface bond stress. When the distance between two points and the strain between two points are known,

the average bond stress in this section is calculated by the balance equation, as shown in Fig. 10 (Hu XP,

Peng G, Niu DT et al. (2020) Experimental study on bond properties between early-age concrete and

deformed steel bars. Construction and Building Materials 236(2020):117593.Zhao DB, Pan J, Zhou YW

et al. (2020) New types of steel-FRP composite bar with round steel bar inner core: Mechanical

properties and bonding performances in concrete. Construction and Building Materials

242(2020):118062.).

The equilibrium equation can be obtained from the equilibrium condition of force:

$$\tau_i \pi dx = A d\sigma \tag{1}$$

Then the average bond stress of this section is as follows:

$$\tau_i = \frac{A}{\pi d} \frac{d\sigma}{dx} \tag{2}$$

SFCBs are composed of carbon fiber and steel bars with completely different performance

characteristics, and the stress transfer mechanism between them is very complex. Assuming that the SFCB

is in the elastic stress stage, the fiber and steel core are well bonded, and when there is no relative slip, the

tensile force borne by them is mainly determined by their own elastic modulus and cross-sectional area.

16

The local bonding stress on the two interfaces can be calculated by using the stiffness law of composite materials, and the calculation formula is derived as follows:

$$\tau_{sf_i} = \frac{A_f}{\pi d_{sf}} \frac{d\sigma_f}{dx} + \frac{A_s}{\pi d_{sf}} \frac{d\sigma_s}{dx} \qquad (3)$$

$$\sigma_f = E_f \varepsilon_f \qquad (4)$$

$$\sigma_s = E_s \varepsilon_s \qquad (5)$$

$$A_f = \frac{\pi}{4} d_{sf}^2 - \frac{\pi}{4} d_s^2 \qquad (6)$$

$$A_s = \frac{\pi}{4} d_s^2 \qquad (7)$$

$$\tau_{si} = \frac{A}{\pi d_{sf}} \frac{d\sigma_s}{dx} \qquad (8)$$

In the formula, A_f and A_s are the cross-sectional area (mm^2) of outer carbon fiber of the SFCB and the cross-sectional area (mm^2) of steel core of the SFCB; d_{sf} and d_s are the cross-sectional diameter (mm) of the SFCB and the inner core diameter (mm) of the SFCB steel bar; E_f and E_s are elastic modulus (GPa) of outer carbon fiber of the SFCB and elastic modulus (GPa) of inner core of the SFCB steel bar, respectively. τ_{sfi} and τ_{si} are the microsegment bond stress (MPa) between the SFCB and concrete interface and the micro-segment bond stress (MPa) between the SFCB fiber and steel core interface, respectively. $d\sigma_f$ and $d\sigma_s$ are the stress differences (MPa) at both ends of the outer fiber and the inner core of the steel bar respectively; dx is the space (mm) between the SFCB microsegments.

(a)Steel bars and CFRP bars   (b)SFCB

Fig. 10. Force acting on the micro-element of reinforcement.

17
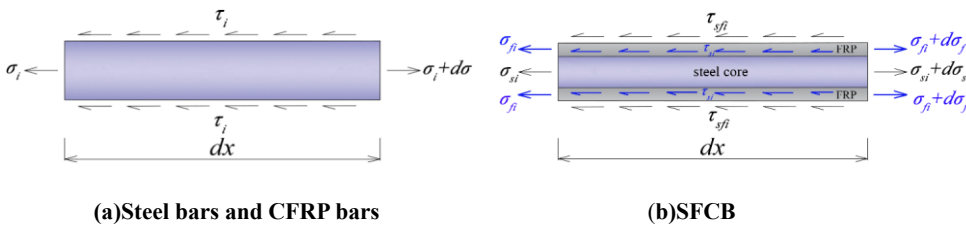
5. Bond stress distribution model

The approximate distribution curve of bond stress can be drawn by calculating the average bond stress at points along the bond length. Obviously, the accuracy of the distribution curve is closely related to the number of control points. The more points there are, the curve is to the actual distribution of bond stress. Previous studies have shown that the bond stress is neither uniformly distributed nor linearly changed along the bond length, and most of them are unimodal or bimodal (Lees J , Burgoyne C . (1999) Transfer bond stresses generated between FRP tendons and concrete. Thomas Telford 51(4):229-239.). There are many factors that affect the distribution and variation of bond stress along the bond length, including the strength of reinforcement, elastic modulus, interface state, concrete strength, constraint conditions, load size and development stage, etc.

In this paper, concrete splitting failure occurred before the steel bar (steel core) yielded, and the relative slip value between the steel bar and concrete was small. It can be seen in Fig. 11 that during the whole loading process, the bond stress presents a bimodal distribution, and the peak position of stress has not changed obviously. The bond stress at the measuring point near the loading end is on the high side, and its value is obviously larger than the average bond stress. With increasing of load, the bond stress of the steel bar specimens increases steadily, while the growth rate of the bond stress between the SFCB and CFRP bars near the loading end decreases, which indicates that obvious bond slip begins to appear near the loading end, resulting in the loss of bond strength.

The bond length has a significant influence on the distribution pattern and law of bond stress. It can be seen in Fig.11 that 1) regardless of the bond length, the bond stress is mainly distributed at 0~0.5 of the relative bond length; 2) with the increase in bond length, the relative position of the bond stress peak is closer to the loading end; and 3) the shorter the bond length, the greater the peak bond stress under the
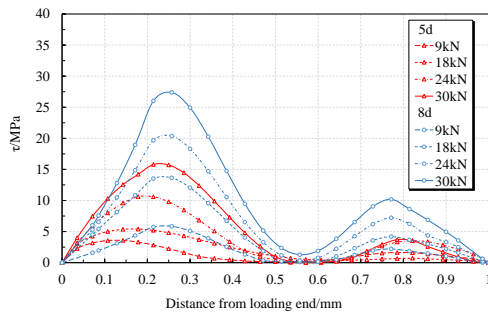
same load. In this paper, the peak bond stress of specimens after 5 d is approximately twice that of specimens after 8 d.
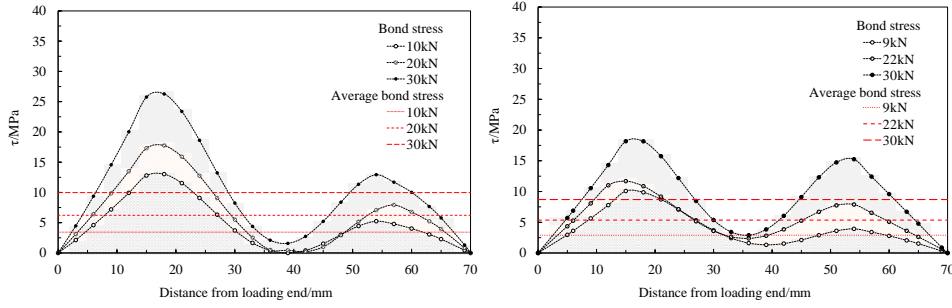
(a)Bond stress distribution curve of S-5d-C80   (b)Bond stress distribution curve of C-5d-C80
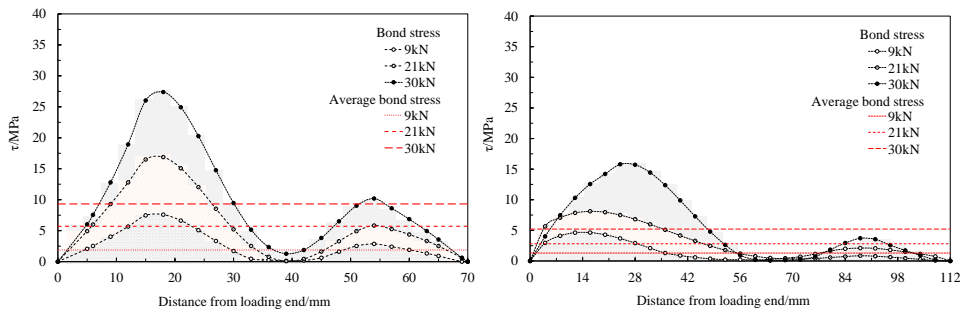
(c)Bond stress distribution curve of SF-5d-C80   (d)Bond stress distribution curve of SF-8d-C80

(e)Comparison between SF-5d-C80 and SF-8d-C80

Fig. 11. Distribution of bond stress along bond length.

The typical bond stress distribution plots of conventional steel rebar and carbon bars are mostly unimodal, as shown in Figure 12. At present, the bond stress distribution models between reinforcement and concrete mainly include: the Burong model (ZHANG B, BENMOKRANE B. (2000) Prediction of Tensile Capacity of Bond Anchorages for FRP Tensions. Journal of Composites for Construction 4(2):39-47.), Jiang model (Jiang TY, Fang Z (2007) Bond Stress Distribution of Bond-type Anchors for CFRP Tendons under the Ultimate Tensile Capacity. Journal of Highway and Transportation Research and Development 2007(12):75-78 92.), and Liu model(Liu YH, Yuan Y. (2011) Bond Stress Distribution Model of Full-thread GFRP Bars in Concrete. Chinese Journal of Underground Space and Engineering 7(S1):1353-1356+1363.) and so on. However, these stress distribution model curves are all unimodal, which lacks applicability to bimodal curves. Therefore, this paper draws lessons from the model analysis of general reinforcement and concrete, and based on the literature (Liu YH, Yuan Y. (2011) Bond Stress Distribution Model of Full-thread GFRP Bars in Concrete. Chinese Journal of Underground Space and Engineering 7(S1):1353-1356+1363.), put forwards the bond stress distribution model under the bimodal curve form, as shown in Formulas (9)~(12):

$$\tau(x) = \frac{x}{x_1} \tau_{p_1} \quad \left(0 < x \le x_1\right) \tag{9}$$

$$\tau(x) = \tau_{p_1} e^{-2\alpha \frac{x - x_1}{d}} \quad \left(x_1 < x \le x_2\right) \tag{10}$$

$$\tau(x) = \frac{x - x_2}{x_3 - x_2} \tau_{p_2} \quad \left(x_2 < x \le x_3\right) \tag{11}$$

$$\tau(x) = \tau_{p_2} e^{-2\alpha \frac{x - x_3}{d}} \quad \left(x_3 < x < L\right) \tag{12}$$

where: τ_{p1} and τ_{p2} are the first and second peak values of bond stress (MPa); x_1, x_2 and x_3 are the coordinates (mm) corresponding to the first bond stress peak, the bond stress peak valley and the second

20

bond stress peak respectively; α is the parameter, which is determined by experiment; d is the diameter (mm) of reinforcement; L is the bonding length (mm).

As shown in Fig.13, the bond stress distribution model proposed in this paper is in good agreement with the experimental data and can be applied to the bond stress of rebar with bimodal distribution. At present, there are few studies on bond stress distribution, and the model proposed in this paper needs to be further verified and improved.
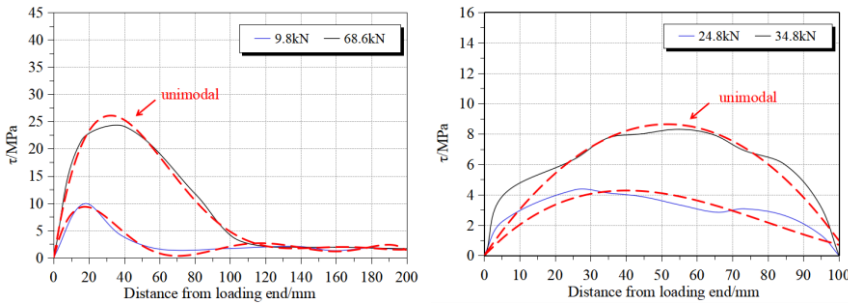
(a)Distribution of CFRP bars bond stress(ZHANG B, BENMOKRANE B. (2000) Prediction of Tensile Capacity of Bond Anchorages for FRP Tensions. Journal of Composites for Construction 4(2):39-47.)(b)Distribution of steel bars bond stress(Liu M, Huang CK, Cheng Y et al. (2006) Test and research on distribution of bond stress of reinforcement and grout concrete. Journal of Liaoning Technical University 2006(05):705-707.)

Fig. 12. Typical bond stress distribution plots of conventional steel rebar and carbon bars.
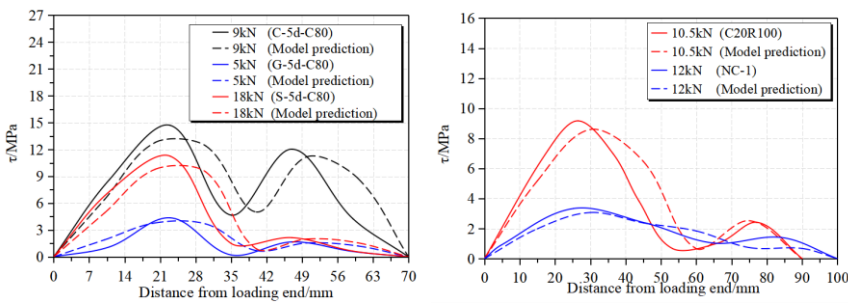
(a)Validate against test results of this paper   (b)Validate against test results of references(Wang

B, Bai GL, Li J et al. (2012) Experimental and the Theoretical Analysis of Bond Stress Distribution

Between the Rebar and the Recycled Concrete. Industrial Construction 42(04):10-14.) (Xu SL, Wang

HC (2008) Experimental Study on Bond-Slip Between Ultra High Toughness Cementitious Composites

and Steel Bar. Engineering Mechanics 2008(11):53-61.)

Fig. 13. Verification of bond stress distribution model.

6.   Conclusion

(1) In the central pull-out tests, the tensile strain of the rebar decreases from the loading end to the

free end along the bond direction, and the first half near the loading end decreases rapidly, while the change

in the second half gradually slows down. At the same time, the specimens with different reinforcement

types and different bond lengths show obvious differences. Under the same bonding conditions, influenced

by the elastic modulus of the materials, under the same load, the tensile strain of the CFRP bars is greater

than that of the SFCB, and the strain of steel bars is the smallest, and the difference increases gradually

with increasing of load. The loading end strain of the SCFCB is able to increase by approximately 40%

over normal reinforcement. The shorter the bond length of reinforcement is, the faster the strain curve

decreases.

(2) The SFCB steel core strain and outer carbon fiber strain have the same growth trend and speed

with the increase of load, but with increasing of load, the steel core strain value is smaller than the carbon

fiber strain at the same position, showing a certain hysteresis.

(3) The bond stress between the reinforcement and concrete is neither evenly distributed nor linearly

decreased along the bond length. In this paper, the bond stress is mainly distributed at 0~0.5 of the relative

bond length. The shorter the bond length, the greater the peak bond stress under the same load. Compared with steel bars and CFRP bars, the bond stress distribution between SFCB and concrete is more uneven, which is mainly reflected in the large difference of bond stress at the double peaks; Similar to CFRP bars, with the increase of load, the growth rate of bond stress between SFCB and concrete near the loading end decreases.

(4) The bond stress distribution model proposed in this paper is in good agreement with the experimental data and can be applied to the bond stress of rebar with a bimodal distribution.

Research significance

It is the first time Bragg grating sensing technology is used to investigate the bond stress of SFCP reinforced concrete. A new bond stress model and a new bond distribution model are also developed.

Acknowledgements

References

Canadian Standard Association (2002) CSA S806 02 Design and construction of building components with fiber reinforced polymers. Toronto, Canada: Canadian Stands Association International.

Fahmy M F M , Abd-Elshafy Z E , Wu Z . (2017) Experimental and Numerical Evaluation of the Shear Behavior of Reinforced Concrete T-Beams with Hybrid Steel-FRP Stirrups. Journal of Composites for Construction 21(4):04017007.1-04017007.18.

Gao D, Huang Y, Chen G et al. (2020) Bond stress distribution analysis between steel bar and steel fiber reinforced concrete using midpoint stress interpolation method. Construction and Building Materials 260:119866.

Gu XL, Chen ZY and Farhad Ansari (2000) Embedded Fiber Optic Crack Sensor for Reinforced Concrete Structures. Structural Journal 97(3): 468-476.

HILL K.O, MELTZ G. (1997) Fiber Bragg grating technology fundamentals and overview. Journal of Lightwave Technology: A Joint IEEE/OSA Publication 15(8):1263-1276.

Hu XP, Peng G, Niu DT et al. (2020) Experimental study on bond properties between early-age concrete and deformed steel bars. Construction and Building Materials 236(2020):117593.

Huang X, Jin ZK and Shen Q (2021) New Method of Temperature and Strain Decoupling Based on Directivity of Fiber Bragg Grating Sensing. Journal of Physics: Conference Series 2101(1):19-20.

Hwang H J , Park H G , Yi W J et al. (2017) Development Length of Standard Hooked Bar Based on Non-Uniform Bond Stress Distribution.   ACI Structural Journal 114(6) : 1637-1648.

Jiang TY, Fang Z (2007) Bond Stress Distribution of Bond-type Anchors for CFRP Tendons under the Ultimate Tensile Capacity. Journal of Highway and Transportation Research and Development 2007(12):75-78 92.

Jiang TY, Fang Z (2010) Bond Stress Distribution of CFRP Tendon in Reactive Powder Concrete. China Journal of Highway and Transport 23(01):49-57.

L. J. Malvar, N. R. Joshi,J. A. Beran et al. (2003) Environmental Effects on the Short-Term Bond of Carbon Fiber-Reinforced Polymer (CFRP) Composites. Journal of Composites for Construction 7(1):58-63.

Lees J , Burgoyne C . (1999) Transfer bond stresses generated between FRP tendons and concrete. Thomas Telford 51(4):229-239.

Liu M, Huang CK, Cheng Y et al. (2006) Test and research on distribution of bond stress of reinforcement and grout concrete. Journal of Liaoning Technical University 2006(05):705-707.

Liu YH, Yuan Y. (2011) Bond Stress Distribution Model of Full-thread GFRP Bars in Concrete. Chinese Journal of Underground Space and Engineering 7(S1):1353-1356+1363.

Malvar L J, Cox J V and Cochran K B (2003) Bond between Carbon Fiber Reinforced Polymer Bars and Concrete I:Experimental Study. Journal of Composites for Construction 7(2):154-163.

Pan J (2016) Research progress on fabrication technique and tensile performance of FRP-Steel composite bar. Journal of Civil and Environmental Engineering 38(S2):18-20.

Pan WH , Tao MX , Nie X et al. (2018) Rebar Anchorage Slip Macromodel Considering Bond Stress Distribution: Monotonic Loading and Model Application. Journal of Structural Engineering 144(8):04018097.

Shi LZ, Zhang JR (2014) Experimental Study on Anchorage Performance of Chemical Adhesive Steel Bar in Concrete. Applied Mechanics & Materials 578-579(2014):331-334.

Sun ZY, Tang Y, Luo YB et al. (2017) Mechanical Properties of Steel-FRP Composite Bars under Tensile and Compressive Loading. International Journal of Polymer Science 2017(1):5691278-1-5691278-11.

Sun ZY, Tang Y, Luo YB et al. (2017) Mechanical Properties of Steel-FRP Composite Bars under Tensile and Compressive Loading. International Journal of Polymer Science 2017(1):5691278-1-5691278-11.

Sun ZY, Wu G, Wu ZS et al. (2009) Experimental Study on the Bond Behavior between Steel Fiber Composite Bar (SFCB) and Concrete. Earthquake Resistant Engineering and Retrofitting 31(01):21-27.

Tang GN (2013) Application study on FBG sensor applied to hull structure health monitoring. MSc thesis,Wuhan University of Technology, Wuhan city, Hubei Province, China (in Chinese).

Wang B, Bai GL, Li J et al. (2012) Experimental and the Theoretical Analysis of Bond Stress Distribution Between the Rebar and the Recycled Concrete. Industrial Construction 42(04):10-14.

Wang L , Zhang JW , Huang CS et al. (2020) Comparative Study of Steel-FRP, FRP and Steel-Reinforced Coral Concrete Beams in Their Flexural Performance. Materials 13(9)：2097.

Wang L, Shen N, Zhang MM et al. (2020) Bond performance of Steel-CFRP bar reinforced coral concrete beams. Construction and Building Materials 245(Jun.10): 118456.1-118456.11.

Wang L, Zhang JW, Chen W et al. (2020) Short term crack width prediction of CFRP bars reinforced coral concrete. Engineering Structures 218(Sep.1)：110829.1-110829.12.

Wu G, Luo YB, Wu ZS et al. (2010) Experimental and Theoretical Studies on the Mechanical Properties of Steel-FRP Composite Bars. China Civil Engineering Journal 43(03):53-61.

Xu SL, Wang HC (2008) Experimental Study on Bond-Slip Between Ultra High Toughness Cementitious

Composites and Steel Bar. Engineering Mechanics 2008(11):53-61.

Xu YL, Shen WD and Wang H (1994) An Experimental Study of Bond-Anchorage Properties of Bars in Concrete. Journal of Building Structures 1994(03):26-37.

Xu YQ (2015) Resarch on Basic Properties of Steel Fiber Composite Bars Reinforced Marine Sand Concrete Beams. MSc thesis,Southeast University Nanjing city, Nanjing city, Jiangsu province, China (in Chinese).

ZHANG B, BENMOKRANE B. (2000) Prediction of Tensile Capacity of Bond Anchorages for FRP Tensions. Journal of Composites for Construction 4(2):39-47.

Zhang LL (2011) Study on Bond Behavior between Steel-FRP Composite Bar (SFCB) and Concrete under Cyclic Loading. MSc thesis,Southeast University, Nanjing city, Jiangsu province, China (in Chinese).

Zhang MM (2019) Experimental study on the bonding properties of steel-carbon fiber composite bars with all-coral concrete. MSc thesis,Guilin University of Technology,Guilin city, Guangxi province, China (in Chinese).

Zhao DB, Pan J, Zhou YW et al. (2020) New types of steel-FRP composite bar with round steel bar inner core: Mechanical properties and bonding performances in concrete. Construction and Building Materials 242(2020):118062.

Zhao WL, Yao ZB, Yu QB et al. (2019) Experimental Study on Bond Anchorage Behavior between Deformed Steel Bar and Lightweight Concrete. Building Structure 49(04):70-75.

Zheng BL, Li W, Zhang WW et al. (2004) Mechanics Behavior of FRP Wrapped Rebar Reinforced Concrete Ⅱ: Mechanic Tests. Acta Materiae Compositae Sinica 21(3):79-83.

List of Table

Table 1． Concrete mix ratio and basic mechanical performance parameters.

Water cement ratio	Cement (kg/m³)	Fly ash (kg/m³)	Mineral powder (kg/m³)	Sand (kg/m³)	Coarse aggregate (kg/m³)	Water (kg/m³)	Water reducer (kg/m³)	Cube Compressive strength (MPa)	Axial compressive strength (MPa)	Tensile splitting strength (MPa)	Young's Modules (GPa)
0.27	404	69	104	720	1100	156	1.731	83.2	53.5	5.3	39.8

Table 2． Mechanical properties of bars.

Bar Type	Bar diameter (mm)	Steel core diameter (mm)	Rib height (mm)	Rib width (mm)	Rib spacing (mm)	Yield strength (MPa)	Bar Young's Modules (GPa)	Ultimate strength (MPa)	Outer fibre Young's Modules (GPa)	Steel core Young's Modules (GPa)
SCFRP	14	8	0.55	10.41	13.37	344.8	150.2	1102.3	127.3	197.4
CFRP	14	—	1.22	10.28	13.84	—	131.6	1102.3	—	—
steel bar	14	—	1.11	2.89	8.35	393.2	205.0	644.4	—	—

List of Figures

26

Fig. 12. Typical bond stress distribution plots of conventional steel rebar and carbon bars.

Fig. 13. Verification of bond stress distribution model.

Fig. 1. Test bars.

Fig. 2.Schematic diagram of the specimens.

Measuring points on steel bar and CFRP bar: a_1、a_2、a_3、a_4、a_5、a_6
Measuring point on fiber: c_1、c_2、c_3、c_4、c_5、c_6
Measuring point on steel core: s_1、s_2、s_3、s_4、s_5、s_6
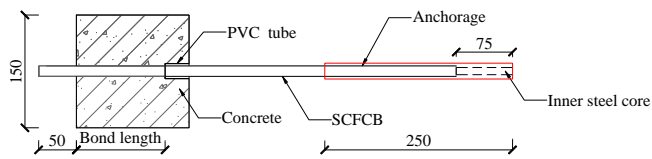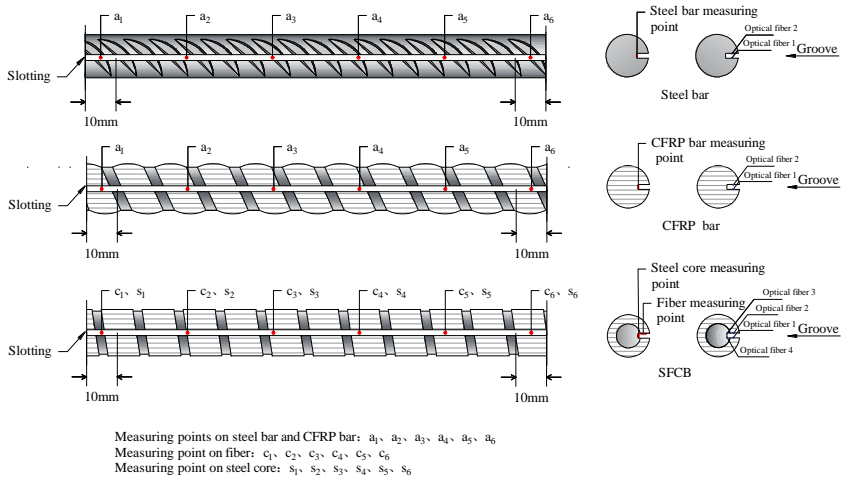
Fig. 3. Fiber Bragg grating measuring point layout.
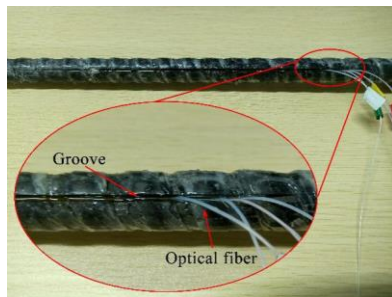
Fig.4. Physical drawing of fiber grating embedding
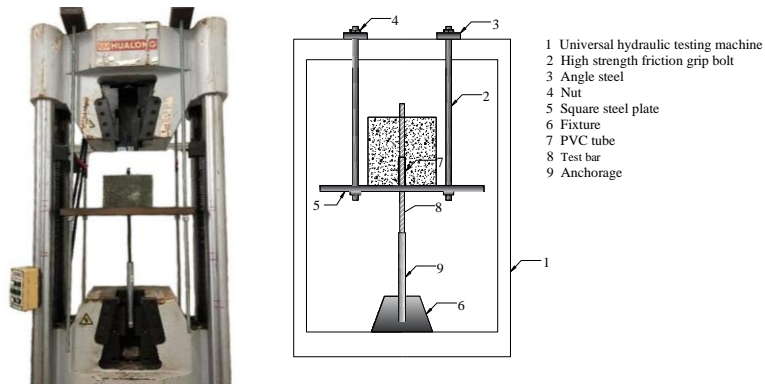
Fig. 5. Schematic diagram of pull-out test equipment.

1 Universal hydraulic testing machine
2 High strength friction grip bolt
3 Angle steel
4 Nut
5 Square steel plate
6 Fixture
7 PVC tube
8 Test bar
9 Anchorage

(a) C-5d-C80

(b) SF-8d-C80

Fig. 6. Failure mode of bond.
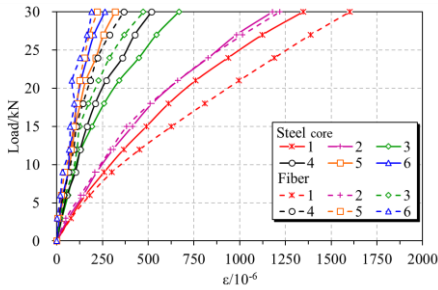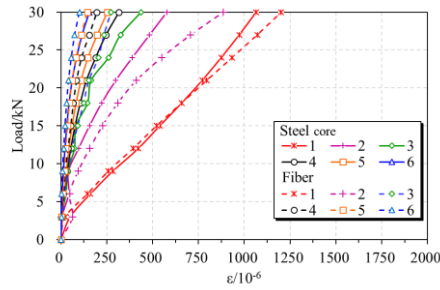
(a)Load-strain curve of SF-5d-C80   (b)Load-strain curve of SF-8d-C80

Fig. 7. Load-strain curve of SFCB steel core and outer fiber.

Note: The positions of measuring points are set according to Figure 3. From the loading end to
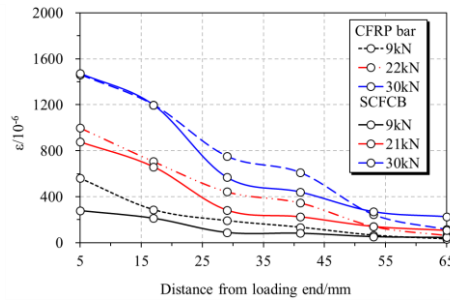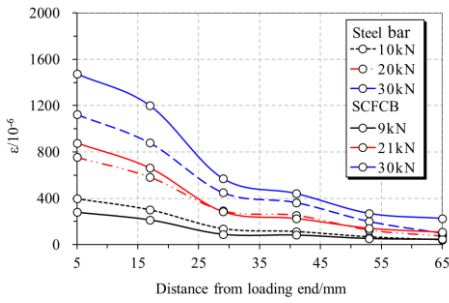
the free end, the measuring point numbers are 1, 2, 3, 4, 5 and 6 in turn.

(a)Comparison between SFCB and steel bars (b)Comparison between SFCB and CFRP bars

Fig. 8. Influence of reinforcement type on strain distribution.
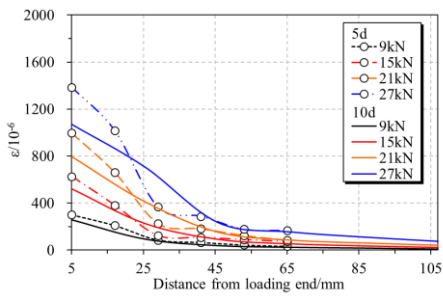
(a)SFCB steel core strain   (b)SFCB outer carbon fiber strain
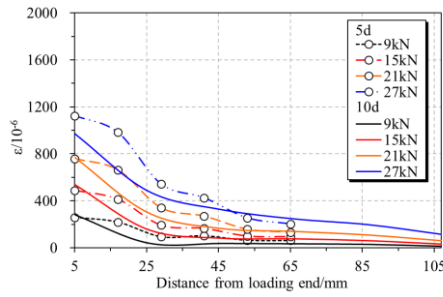
Fig. 9. Influence of bond length on strain distribution.
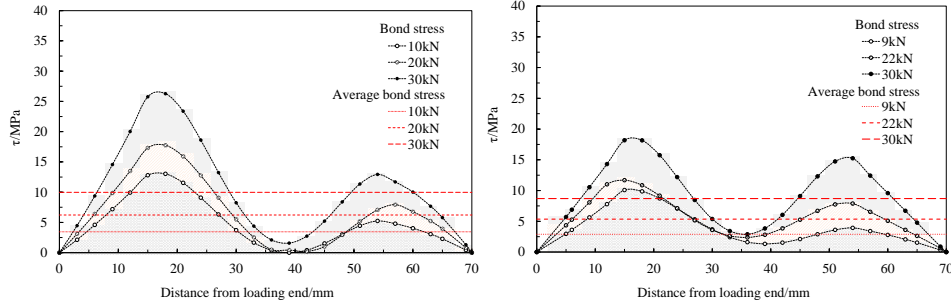
(a)Bond stress distribution curve of S-5d-C80

(b)Bond stress distribution curve of C-5d-C80
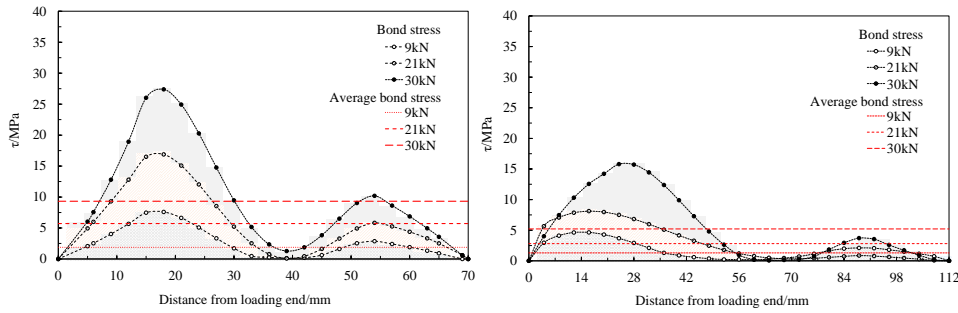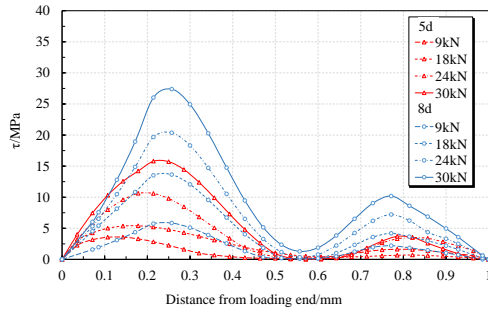

(c)Bond stress distribution curve of SF-5d-C80

(d)Bond stress distribution curve of SF-8d-C80
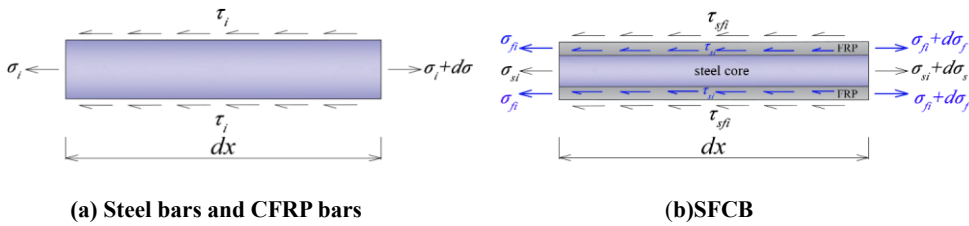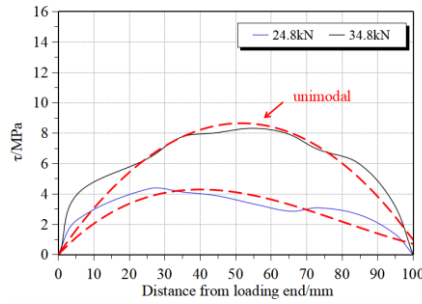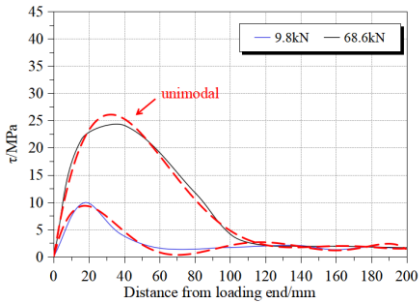

(a) Steel bars and CFRP bars

(b)SFCB

Fig. 10. Force acting on the micro-element of reinforcement.

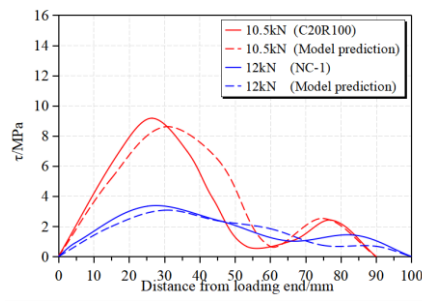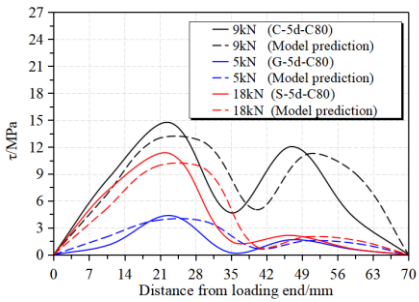**(e)Comparison between SF-5d-C80 and SF-8d-C80**

Fig. 11. Distribution of bond stress along bond length.

(a)Distribution of CFRP bars bond stress[33]   **(b)Distribution of steel bars bond stress[34]**

Fig. 12. Typical bond stress distribution plots of conventional steel rebar and carbon bars.

(a)Validate against test results of this paper   **(b)Validate against test results of references**

[16], [35]

Fig. 13. Verification of bond stress distribution model.